ELSEVIER

Surface Science 417 (1998) 301–310

surface science

Direct observation of subsurface oxygen on Rh(111)

J. Wider, T. Greber *, E. Wetli, T.J. Kreutz, P. Schwaller, J. Osterwalder

Physik-Institut, Universität Zürich, Winterthurerstrasse 190, CH-8057 Zürich, Switzerland

Received 22 May 1998; received in revised form 8 August 1998; accepted for publication 8 August 1998

Abstract

A Rh(111) surface has been exposed to oxygen under conditions that favour the formation of a subsurface oxygen species. After exposure to 10^5 L O_2 at a surface temperature of 470 K X-ray photoelectron diffraction data of O 1s emission reveal that (5 ± 2)% of a monolayer of oxygen atoms occupy octahedral interstitial sites just underneath fcc adsorption sites. The occupation of such a site forces the oxygen atoms adsorbed in its close vicinity to switch from the stable fcc site to the hcp adsorption site. Implications of this finding for the interpretation of temperature-programmed desorption spectra, as well as for the catalytic behaviour of the oxidized Rh(111) surface, are discussed. © 1998 Elsevier Science B.V. All rights reserved.

Keywords: Rhodium; Subsurface oxygen; Surface structure; X-ray photoelectron diffraction; X-ray photoemission spectroscopy

1. Introduction

In heterogenous catalysis the surface takes the role of breaking molecular bonds and of increasing the reaction probability because adsorbed species diffuse in two rather than three dimensions. For both processes only adsorbed molecular or atomic species on top of the surface are relevant. Recent experiments have indicated, however, that "subsurface species" alter the catalytic activity [1–8]. In the case of metal oxygen systems, subsurface oxygen is a mobile oxygen species that is dissolved in the metal. It is different from stable oxides that can be formed as well in the metal $+ O_2$ reaction [9]. Unfortunately, these subsurface species have been rather elusive in attempts to observe them directly. This might be because they occur in high concentrations only under pressure/temperature conditions where structure-sensitive surface techniques can no longer be applied, while their concentration is low under ultrahigh vacuum (UHV) conditions.

In the O/Rh(111) system, indirect evidence for the participation of subsurface oxygen in surface reactions comes from temperature-programmed desorption spectroscopy (TDS) experiments [1,5]. Room temperature (RT) exposure to O_2 leads to an ordered (2×1)-1O structure at a saturation coverage of 0.5 monolayer (ML), and a broad TDS spectrum ranging from 650 to 1200 K is found. O_2 exposure at elevated temperature (higher than 400 K) leads to a distinct feature in the TDS spectrum at 720 K, which grows with increasing exposure. This low binding energy oxygen state was attributed to subsurface oxygen, because He atom scattering showed no significant changes in the surface periodicity when the surface was charged with extra oxygen to produce this TDS peak [5]. This assignment implies an efficient desorption channel for subsurface oxygen that

* Corresponding author. E-mail: greber@physik.unizh.ch

0039-6028/98/$ – see front matter © 1998 Elsevier Science B.V. All rights reserved.
PII: S0039-6028(98)00674-8

comprises recombination with a second oxygen on top of the surface.

In order to shed new light on this issue, we present an X-ray photoelectron diffraction (XPD) study of the O/Rh(111) system. XPD is a local structure probe which is very sensitive to subsurface species [10–12]. The angle-dependent O 1s photoemission signal from a Rh(111) surface exposed to large amounts of O_2 at elevated temperatures comprises contributions both from oxygen adsorbed on the surface and from subsurface oxygen. While the adsorbate produces a rather isotropic emission pattern, subsurface emitters produce strong scattering features due to forward focusing by surface layer Rh atoms and by adsorbate atoms. Subsurface concentrations in the percent of a monolayer range can thus be detected by this method.

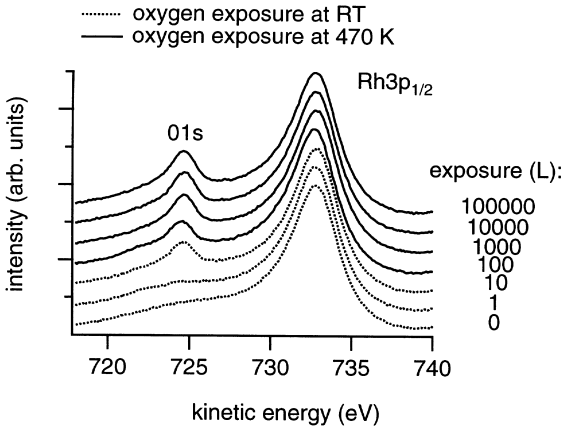

Fig. 1. XPS spectra exicted by Mg Kα radiation ($\hbar\omega = 1253.6$ eV) obtained after different oxygen exposures at room temperature and at 470 K. The Rh $3p_{1/2}$ peak was used as a reference to normalize the spectra.

2. Experimental

The experimental setup, consisting of a VG ESCALAB 220 photoelectron spectrometer and a computer-controlled two-axis goniometer, has been described elsewhere [13]. A Rh(111) single crystal has been mechanically polished and then cleaned in UHV by repeated cycles of Ar^+ bombardment (1.5 kV down to 0.2 kV) at 440 K and annealing at 780 K. Sample cleanness was verified by X-ray photoelectron spectroscopy (XPS, less than 0.1 ML carbon contamination), and its crystallinity by low-energy electron diffraction (LEED). O_2 exposures were done at room temperature or at 470 K, and coverages measured by taking Mg Kα excited O 1s to Rh $3p_{1/2}$ core level intensity ratios (Fig. 1). An exposure of 10 L (1 L = 1 Langmuir = 1.33×10^{-6} mbar s) O_2 at room temperature leads to a (2×2) LEED pattern. At 10 L exposure the oxygen uptake as measured by XPS exhibits a first saturation level. If we determine the coverage at this level by means of the O:Rh XPS intensity ratio, the corresponding photoemission cross sections and the electron mean free path (10 Å at 700 eV [14]) a coverage $\Theta_{XPS} = 0.43 \pm 0.05$ ML is found. This is close to the value of Schwegmann et al. [15] who calibrated the 10 L coverage by means of a combined Auger electron spectroscopy (AES)/LEED study to a value of 0.5 ML. We therefore favour the calibration of Schwegmann et al. above that of another study [16] which calibrates the 10 L exposure with $\Theta = 0.25$ ML. This assignment is also supported by recent total energy calculations that favour a saturation coverage of 0.5 ML over 0.25 ML [17]. To obtain absolute coverages (Fig. 2) we thus associated the 10 L exposure to 0.5 ML. TDS data showed a similar behaviour with varying O_2 exposure as has been described in the literature [1,5],

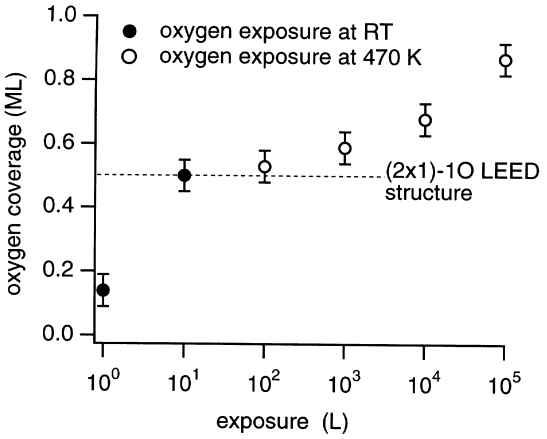

Fig. 2. Oxygen coverage curve obtained from the data of Fig. 1. A first saturation is reached at 10 L, in agreement with Ref. [15].

with the characteristic shift of the oxygen peak towards lower desorption temperatures when the surface is exposed to larger amounts of O_2 at elevated temperature.

In order to get a good signal to noise ratio in the XPD data the angular resolution was set to $(5.0 \pm 0.5)^\circ$ FWHM and the energy resolution to 1.2 eV FWHM. XPD measurements of full hemispherical O 1s intensity patterns take about 5 h. Measurements at room temperature and a background pressure of typically 5×10^{-10} mbar showed the surface oxygen layer to become gradually depleted due to reaction with residual gas (mostly H_2 and CO). Cooling the crystal to 190 K during the measurement proved to keep the adsorbate layer more or less stable, with a small contribution due to CO accumulating over the measuring time.

Each XPD plot presented in the following shows the intensity in a linear grayscale of a particular core level (O 1s or Rh $3d_{5/2}$) along typically 5000 emission angles into the hemisphere above the surface. The emission angles are stereographically projected where the centre of the plot corresponds to normal and the circumference to grazing emission [18]. Data are recorded from grazing ($\theta = 88^\circ$) to normal ($\theta = 0^\circ$) emission. In order to account for the low emission intensity parallel to the surface that is caused by refraction effects and the instrumental response function the individual azimuthal scans have been normalized by a procedure described in Ref. [19].

3. Results

3.1. Reference case: the (2×1)-1O adsorbate structure

The adsorbate structure formed at 273 K exposure to O_2 at saturation (10 L) has been characterized by Schwegmann et al. [15]. They find a (2×1)-1O structure with rows of oxygen atoms adsorbed in fcc sites and occurring in three rotated domains. We have used this structure as a reference both for our coverage scale (Fig. 2) and for the XPD pattern of a complete adsorbate layer with no subsurface oxygen present. In Fig. 3a an Rh $3d_{5/2}$ XPD pattern is shown. The overall anisotropy, defined as $A = (I_{max} - I_{min})/I_{max}$ is 0.29 in this data. Because of the forward scattering nature of photoelectron diffraction, such substrate patterns reflect directly the crystal directions and its orientation [20].

The O 1s diffraction pattern (Fig. 3b) is very different. In producing this plot, the spectral background had to be carefully subtracted from the O 1s signal, because it is well known to carry the angular signature of the higher kinetic energy Rh $3p_{1/2}$ peak [21]. The O 1s pattern has a reduced anisotropy of 0.19. Its most eye-catching features are three dark ring-like features centred at a polar angle of $\theta = 64^\circ$. These dark rings are due to destructive interference and represent cuts across backscattering cones along the O–Rh axes. From the centre of the ring and its diameter we are able to determine the angle between the surface normal and the O–Rh axis, which in this case turns out to be $\theta = 50^\circ$ [22]. Other characteristic features are three high intensity patches on the constructive interference backscattering cones at 82° polar angle, six maxima at very grazing angles, i.e. at the rim of the pattern, and various thin lines of higher intensity.

Such adsorbate diffraction patterns can be interpreted rather directly by considering simple emitter–scatterer configurations [23]. If we consider photoemission from a particular oxygen site, and if we take only one neighbour atom for elastic scattering, the two atoms define an axial symmetry with a forward scattering peak along the emitter–scatterer direction and circles of reduced or enhanced intensities around this axis whenever the scattered and unscattered waves are out of phase or in phase with each other. At 88° polar angle the diffraction anisotropy is 0.19. The six maxima for grazing angles are thus identified with forward scattering along oxygen–oxygen directions within the adsorbate layer. For clarification, one of these directions is indicated in Fig. 3b and c. First-order constructive interference fringes are just barely visible as thin lines crossing the same azimuth near $\theta = 60^\circ$.

Forward focusing maxima are absent for polar angles further from the surface, consistent with the structural model of a true adsorbate structure

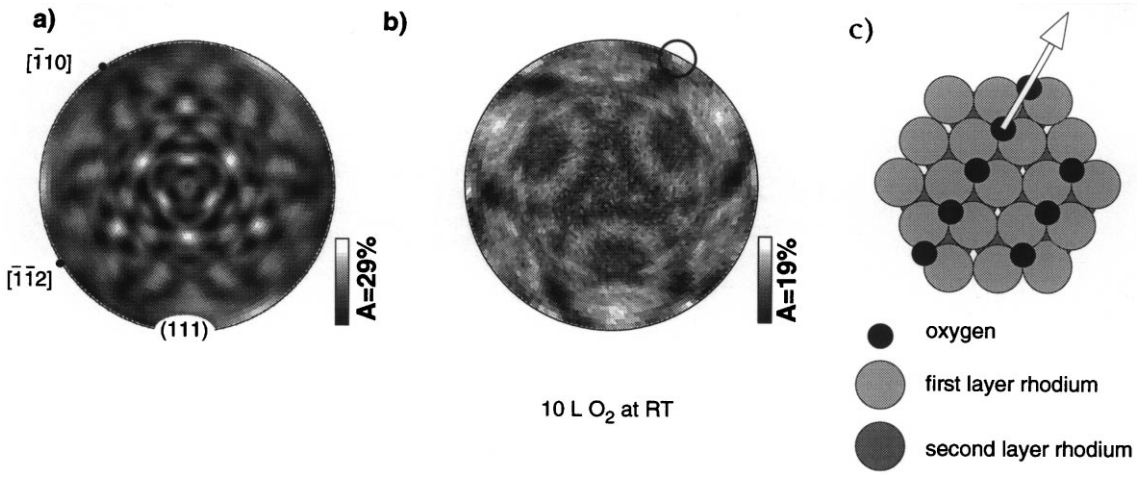

Fig. 3. Mg Kα ($\hbar\omega = 1253.6$ eV) excited Rh $3d_{5/2}$ ($E_{kin} = 947$ eV) XPD pattern from the clean Rh(111). (b) Experimental O 1s ($E_{kin} = 723$ eV) XPD pattern at 10 L O_2 (exposed at room temperature), which corresponds to 0.5 ML. This data has been threefold averaged. Note the three ring-like features which are due to backscattering off the nearest neighbour Rh atoms right below the oxygen adsorbate. (c) Cluster consisting of two layers of Rh and one domain of the (2×1)-1O oxygen overlayer structure. The oxygen atoms are occupying fcc sites.

with atoms adsorbed above the surface layer. The three ring-like structures show no forward scattering maximum in their centre and they can therefore not be identified with first-order interference fringes. The circular shape still indicates a simple one-scatterer origin and suggests that these rings are due to backscattering off the Rh nearest neighbours right below the oxygen adsorbate. The three high intensity patches on the constructive interference backscattering cones at 82° polar angle still have to be discussed. Forward scattering from oxygen emitters that are e.g. located at steps is not likely to cause the high intensities since we would expect for three equivalent steps a sixfold pattern. There are, however, indications that the zero-point motion of the oxygen atoms vertical to the surface causes a pile up of diffraction intensity at 82° polar angle and that furthermore the first-order diffraction pattern of the O–O scattering also contributes to this high intensity.

In order to verify the observation of backscattering we have performed single-scattering cluster (SSC) calculations [10,24] for small clusters with one O atom adsorbed in either an fcc or hcp threefold hollow site and for a bond distance as taken from the analysis of Schwegmann et al. [15]. From the comparison of the two resulting patterns with the respective cluster geometries (Fig. 4b and d we can identify the ring-like features with constructive interference of the primary O 1s photoelectron wave and its counterpart scattered off a nearest-neighbour Rh atom in a near-backscattering geometry (Fig. 4e). Clearly, these features also show up in the experimental data of Fig. 3b, and their arrangement permits an easy and unambiguous assignment of the local bonding site, which is of the fcc type in agreement with Ref. [15]. This strong appearance of backscattering features in angle-scanned XPD is new, and we shall elaborate further on the potentialities of such features for direct structure determination elsewhere [22]. Here, we just use this data in order to have a well-defined reference frame for the clean adsorbate case in our search for subsurface species.

3.2. Observation of subsurface oxygen

In order to favour the formation of subsurface oxygen we raised the temperature during oxygen exposure to 470 K. Fig. 1 shows the spectral region of Rh $3p_{1/2}$ and O 1s emission for a number of different oxygen exposures. The oxygen signal saturates at 10 L, as observed in other studies [15]. Much higher exposures at elevated temperature

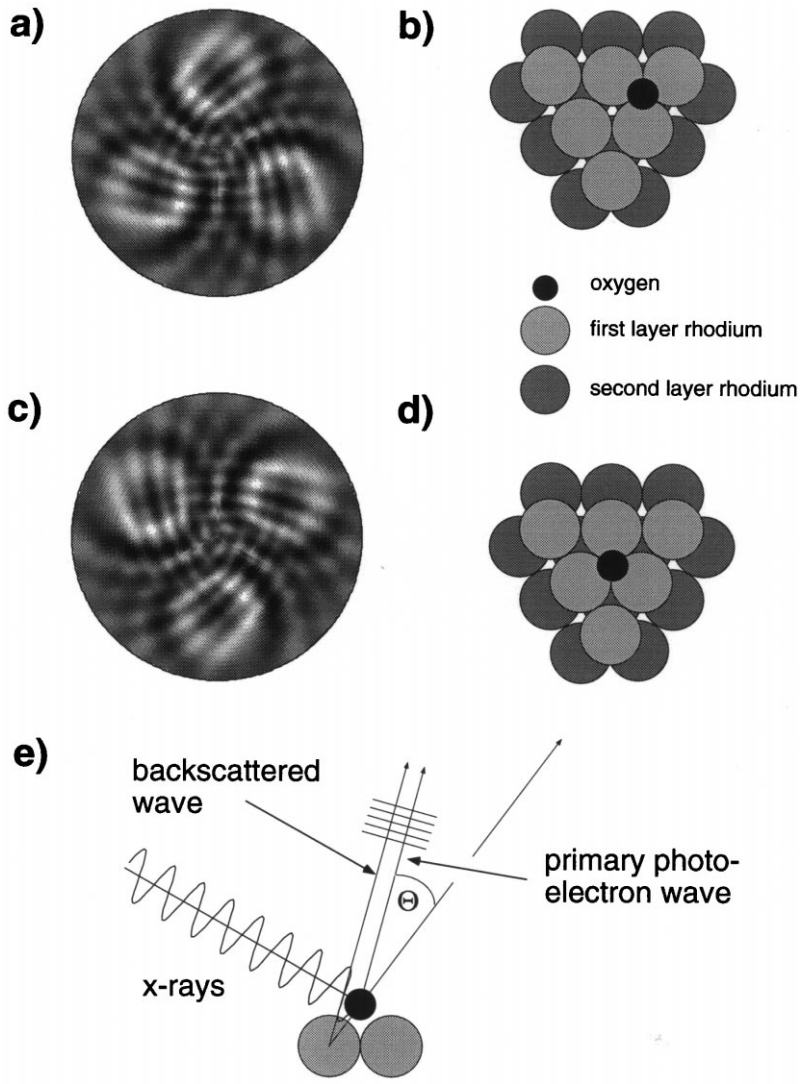

Fig. 4. (a) Single scattering cluster (SSC) calculation for an overlayer structure where the oxygen atoms occupy hcp sites. (b) Corresponding cluster, consisting of two layers of Rh and one adsorbate oxygen atom. Only the three nearest-neighbour Rh atoms have been included in the calculation. (c) and (d) Same as (a) and (b), now with the adsorbate oxygen atoms occupying fcc sites on the Rh surface. (e) Schematic illustration of the backscattering process. The primary photoelectron wave and the backscattered wave are interfering, which leads to the ring-like features in the patterns (a) and (c).

lead to a marked increase, which reflects itself in the coverage versus exposure curve as shown in Fig. 2.

In Fig. 5 the O 1s XPD patterns for exposures of 10^3, 10^4 and 10^5 L are shown. They are all rather similar in appearance, and also resembling the 10 L adsorbate pattern of Fig. 3b. While the anisotropies remain more or less consistent (0.15, 0.17, 0.15) for 10^3, 10^4 and 10^5 L, the intensities for normal emission increase. From this it is concluded that the oxygen coverage increases (0.59, 0.68, 0.87 ML, see Fig. 2) and that the additional oxygen mainly occupies fcc adsorption sites. On closer inspection one finds distinct features, indicated by arrows in Fig. 5c, that are progressively enhanced with increasing oxygen exposure. To

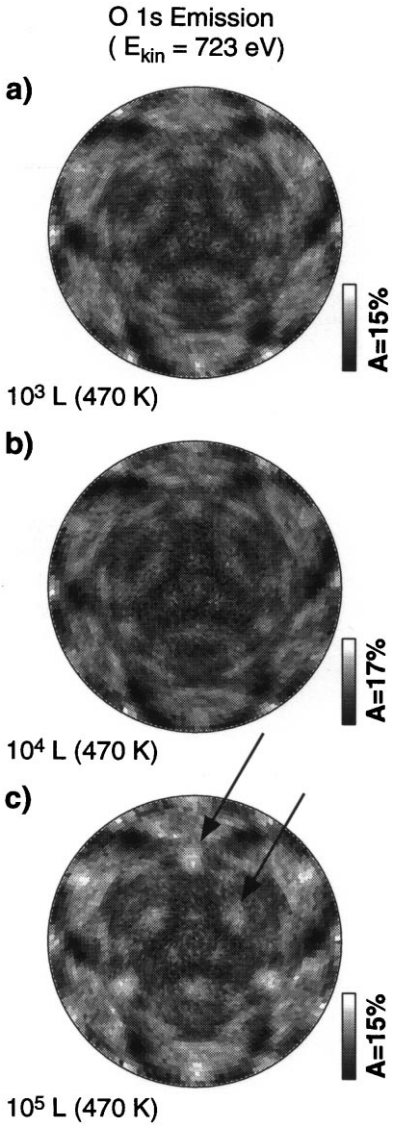

Fig. 5. Experimetal O 1s X-ray photoelectron diffraction patterns for oxygen exposures of (a) 10^3 (b) 10^4 and (c) 10^5 L. The excitation radiation was Mg Kα ($\hbar\omega = 1253.6$ eV) and the exposures were carried out at a crystal temperature of 470 K. In all patterns we see the three ring-like features and in (c) we note in addition the appearence of six forward scattering maxima (indicated with arrows) which are only vaguely visible at lower oxygen exposures.

follow the growth of these maxima more quantitatively circular sections through these data, i.e. azimuthal scans of O 1s intensity at a polar angle of $\theta = 58^\circ$ are given in Fig. 6. We note that through-

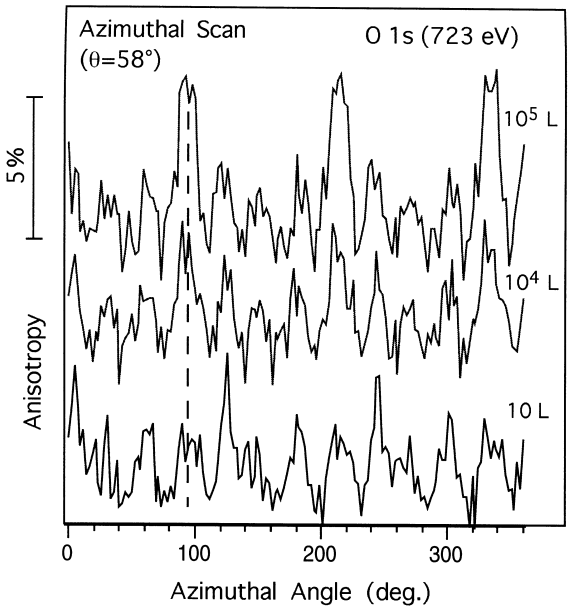

Fig. 6. Circular cuts through the patterns of Fig. 5 at a polar angle of $\theta = 58^\circ$. The peaks at azimuthal angles of $\phi = 100^\circ$, $\phi = 220^\circ$ and $\phi = 340^\circ$ are increasing with increasing oxygen exposure.

out these raw data overall anisotropies are below 5%, which makes these experiments rather demanding. At azimuthal positions near $\phi = 100^\circ$, 220° and 340° clear maxima grow in, reaching anisotropy values of 6%.

Since the diffraction pattern at 10^5 L remains more or less unchanged except for these extra features we have strong evidence that the fcc adsorption site still represents the predominant oxygen species. We can suppress their contribution to the pattern by subtracting the reference pattern from the room temperature 10 L preparation. To do this we normalized both diffraction patterns such as to produce fcc site patterns of equal intensities. The resulting difference pattern is shown in Fig. 7a. It consists of a simple threefold arrangement of two distinct sets of maxima, which strongly suggests them to be of forward-scattering origin. Here is thus the evidence for the surface penetration of oxygen.

Simple geometrical arguments place the oxygen atom into an octahedral site between the first and second Rh layer, which lies just underneath the

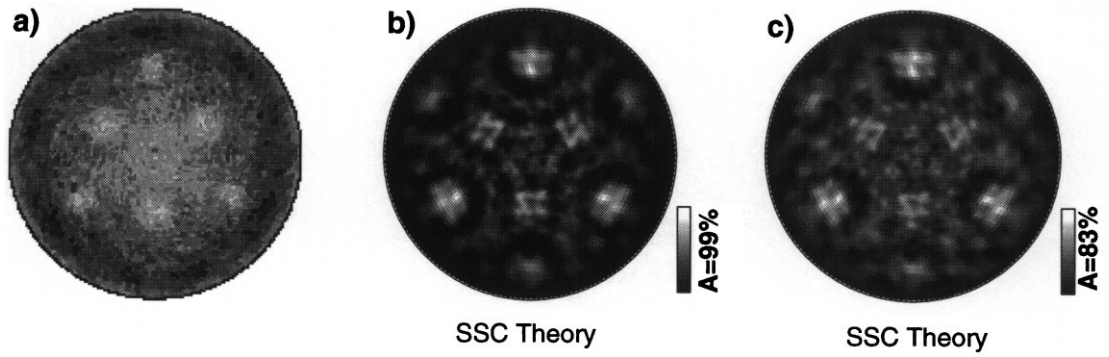

Fig. 7. (a) Diffraction pattern obtained by subtracting the normalized 10 L data from the normalized 10^5 L data in order to expose only the features that are due to the subsurface oxygen and the extra adsorbate oxygen on hcp sites. (b) SSC calculation with photoelectron emission from the octahedral subsurface oxygen. (c) SSC calculation with photoelectron emission from the octahedral subsurface oxygen and the adsorbate oxygen placed on hcp sites. This extra emission causes no additional features in the diffraction pattern. It only reduces the anisotropy of the pattern. The calculations (b) and (c) both reproduce well all of the features seen in (a).

fcc adsorption site (Fig. 8): The outer set of maxima at $\theta = 58^\circ$ represents the forward scattering maxima through the nearest neighbour Rh atoms in the top layer (Fig. 8b). By simple triangulation, and by assuming that the horizontal bond distances are unchanged by the presence of the interstitial oxygen atom, the angle of 58° translates directly into a vertical O–Rh distance of 0.82 Å.

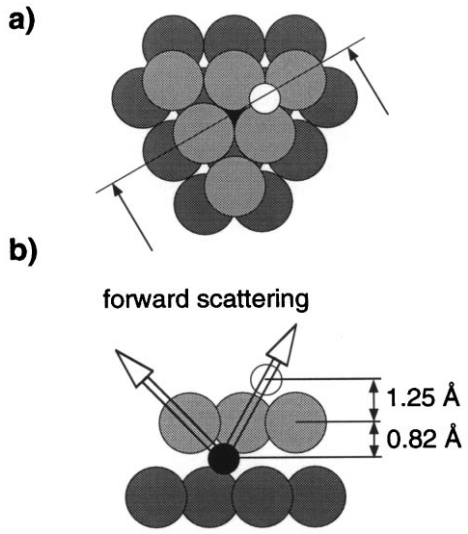

Fig. 8. Top view of the cluster that corresponds to the SSC calculations of Fig. 7b and c. The cluster consists of two layers of Rh, one subsurface oxygen occupying an octahedral interstitial site and one adsorbate oxygen sitting on a hcp site. (b) Vertical cut through the cluster along the line indicated in (a).

The inner set of maxima at $\theta = 38^\circ$ is less obvious to explain, since the nearest neighbour Rh sites are already accounted for, and the occupation of sites further below the surface would lead to a more complicated pattern with more forward scattering directions. We are thus led to the conclusion that these inner maxima are due to forward scattering processes involving adsorbed oxygen atoms. Now, if we had fcc site occupation, a maximum should be observed at normal emission and/or further maxima should appear at polar angles of $\theta = 64^\circ$. Obviously this is not the case. However, if we place oxygen atoms into hcp sites which are just adjacent to the subsurface site (Fig. 8), we obtain just the inner set of forward scattering maxima.

In order to corroborate these findings we performed SSC calculations for small clusters of various geometries. In Fig. 7b the result of a calculation for emission from the octahedral subsurface oxygen with three oxygen atoms in the adjacent hcp sites is shown. In Fig. 7c the emission from one oxygen atom evenly distributed on the three equivalent hcp sites is included as well. It is seen that the oxygen on top of the surface lowers only the overall anisotropy but creates no new XPD features as strong as the forward scattering features of the oxygen in the subsurface site. From the XPD results it is difficult to state how many of the three hcp sites around the occupied octahe-

dral site are occupied by oxygen. In Fig. 8 a corresponding cluster with a subsurface oxygen in the octahedron site and a adsorbed oxygen atom in an adjacent hcp site is shown. The geometry of oxygen in the octahedral and in the hcp site clearly accounts for all features in the experimental difference spectrum. We have verified the uniqueness of this structural model by running SSC calculations for a number of other geometries, including an octahedral site between layers 1 and 2 with fcc adsorption sites occupied and without adsorbed oxygen, an octahedral site between layers 2 and 3 with and without adsorbed oxygen in either fcc or hcp sites, the same combinations for tetrahedral sites, as well as various substitutional sites. Finally we have promoted extra Rh atoms into hcp adsorption sites next to a subsurface site. With none of these geometries we obtained an agreement nearly as good as for the model of Fig. 8. We are thus left with the conclusion that the presence of an oxygen atom in this type of subsurface site changes the surface potential energy for chemisorbed oxygen atoms in its vicinity in such a way as to make the hcp site the more favourable adsorption site.

3.3. Quantification of subsurface site occupation

We have also tried to quantify the absolute number of ordered subsurface oxygen atoms, using both the information from the oxygen coverage (Fig. 2) and that from the XPD anisotropies extracted from Fig. 7a and b. From the SSC calculation (Fig. 7b) we learn that the anisotropy A_{SSC} of the O–Rh forward scattering peaks at $\theta = 58^\circ$ is 80%. From the experimental data of Fig. 6 we know that the observed value is only 6%, i.e. most of the oxygen signal is due to the almost isotropic emission from adsorbate sites, with anisotropy values of less than 5%. In order to extract quantitative concentration values for both subsurface and adsorbed oxygen atoms the following simple model is adopted:

We assume the emission from an adsorbed O atom to be completely isotropic and denote the measured intensity per atom by I_0. For a subsurface site we write $I_m \exp(-L/\Lambda_e)$ for the intensity along the O–Rh forward scattering direction ϕ_m, while we take it to be $I_0' \exp(-L/\Lambda_e)$ in any other arbitrary direction ϕ_0. The factor $\exp(-L/\Lambda_e)$ describes the attenuation due to inelastic scattering where L is the scattering path and Λ_e the inelastic mean free path. For simplicity I_0' is set equal to I_0. The measured intensities along these directions is now:

$$I(\phi_m) = c_{ads} I_0 + c_{sub} I_m \exp(-L/\Lambda_e)$$

and

$$I(\phi_0) = c_{ads} I_0 + c_{sub} I_0 \exp(-L/\Lambda_e)$$

where c_{ads} and c_{sub} are concentrations of adsorbed and subsurface oxygen. From these expressions we can calculate the resulting anisotropy of the maximum at ϕ_m:

$$A = \frac{I(\phi_m) - I(\phi_0)}{I(\phi_m)} = \frac{c_{sub}(I_m - I_0)\exp(-L/\Lambda_e)}{c_{ads} I_0 + c_{sub} I_m \exp(-L/\Lambda_e)}$$

From the SSC calculation for the subsurface site we get a value for the case $c_{ads} = 0$:

$$A_{SSC} = \frac{I_m - I_0}{I_m} \simeq 0.8$$

From the measured anisotropy we thus obtain the concentration ratio as follows:

$$\frac{c_{sub}}{c_{ads}} = \frac{A(1 - A_{SSC})}{A_{SSC} - A} \exp\left(\frac{L}{\Lambda_e}\right)$$

The subsurface photoelectron has a path length L of about 3.8 Å to the surface at $\theta = 58^\circ$, and the inelastic mean free path Λ_e is of the order of 10 Å[14], which yields a value of about 1.4 for the exponential. From these numbers we obtain for a measured anisotropy of 6% a ratio of $c_{sub}/c_{ads} = 0.02$ which is very low. It is an empirical fact that anisotropy values from SSC calculations are too high [10]. If I_m is reduced by a factor of 2 ($A_{SSC} \simeq 0.6$), we still obtain a low subsurface concentration of $c_{sub} = 0.06 c_{ads}$ for this case. This analysis shows that only a small fraction of a monolayer of oxygen has penetrated the surface at 10^5 L exposure, and it also highlights the sensitivity of XPD to such low concentrations.

Can we reconcile this small number with the coverage curve calculated from the O 1s intensities

(Fig. 2)? The coverage increase from 0.5 to 0.9 ML between 10 and 10^5 L exposure, and the preservation of the O 1s XPD pattern characteristic of the fcc adsorption site, means necessarily that additional oxygen is only partially brought into subsurface sites while most of it must be accommodated in the adsorbate layer, progressively filling empty fcc adsorbation sites. A similar analysis as presented for the anisotropies can also be carried out for the O 1s intensities: The normal emission intensities at 10 L and at 10^5 L can be written as

$$I(10\ \mathrm{ML}) = c^0_{\mathrm{ads}} I$$

and

$$I(10^5\ \mathrm{ML}) = c_{\mathrm{ads}} I + c_{\mathrm{sub}} I \exp(-L/\Lambda_{\mathrm{e}})$$

where I is the normal emission intensity for 1 ML of oxygen, c^0_{ads}, c_{ads} and c_{sub} are concentrations of adsorbed oxygen at 10 L (=0.5 ML), at 10^5 L, and the concentration of subsurface oxygen, respectively. The exponential factor describes again inelastic attenuation effects. We have further $I(10^5\ \mathrm{L})/I(10\ \mathrm{L}) = 0.9/0.5$ and $c_{\mathrm{sub}}/c_{\mathrm{ads}} = 0.05 \pm 0.03$ at 10^5 L from the anisotropy analysis. From these numbers we obtain a value of 0.05 ± 0.03 ML for the absolute subsurface oxygen concentration and 0.83 ± 0.05 ML for the adsorbate layer. In the latter case the error bar is mainly determined by the absolute coverage calibration using the (2×1)-1O reference structure, while in the subsurface case the error is determined by the uncertainties in A_{SSC}.

The low concentration of subsurface oxygen makes it impossible to see associated hcp site adsorbates directly by their characteristic backscattering pattern (Fig. 4c). Even if three hcp sites were occupied per subsurface oxygen, we would have roughly 0.1 ML of this species which cannot be observed in a backscattering geometry where anisotropies are of the order of 5% only.

4. Discussion and conclusions

We have established that after extended exposure to oxygen at 470 K and subsequent cooling to 190 K, low concentrations of subsurface oxygen can be stabilized on Rh(111), while the concentration of the adsorbed species rises to 0.8 ML. Together with the findings of Schwegmann et al. [15] and Peterlinz and Sibener [5] the following model for the initial stage of oxidation of Rh(111) can be proposed. After the formation of an oxygen overlayer with a coverage of 0.5 ML and with the oxygen atoms occupying fcc hollow adsorption sites, further oxygen uptake of the surface slows down by kinetic hindering. In thermally activating the substrate to 470 K further oxygen can be adsorbed, though more slowly, in on top adsorption sites where the coverage remains below 1 ML. In this regime atomic oxygen may dissolve into the bulk and the formation of subsurface oxygen in octahedral sites is observed. Interestingly the embedding of oxygen in these sites forces adsorbed oxygen in fcc sites to switch from fcc to hcp hollow sites above the octahedral site. At first this site switch is surprising since it implies that the oxygen–oxygen distance decreases from 2.96 Å in the fcc–octahedron site configuration to 1.99 Å in the hcp–octahedron site configuration. The apparent O–O attraction indicates, on the other hand, that the O–Rh bonding becomes weaker in the subsurface configuration. It is interesting to consider the TDS data [1,5] in view of this structure. The narrow desorption peak near 720 K that arises in the presence of subsurface oxygen might in fact be produced by the oxygen atoms sitting in hcp sites rather than by subsurface atoms directly. Intuitively a picture is drawn where O_2 desorption is initiated by oxygen hopping from the octahedral site to the fcc site on top, meeting a sterically favourable situation for recombination with oxygen in the hcp site. The catalytic properties of this system for reactions involving atomic oxygen can be influenced along the same lines by the presence of subsurface oxygen: the presence of fcc and hcp site occupation in the adsorbate layer should alter the reactivity of this surface, and subsurface oxygen may further act as an additional source of atomic oxygen that can react with chemisorbed molecules.

Acknowledgements

We gratefully acknowledge technical support from W. Deichmann and fruitful discussions with

R. Imbihl, F. Esch, M. Neumann V. Ganduglia-Pirovano and H. Over. This work was supported by the Swiss National Science Foundation.

References

[1] P.A. Thiel, J.T. Yates Jr.,, W.H. Weinberg, Surf. Sci. 82 (1979) 22.
[2] J. Segner, C.T. Campbell, G. Doyen, G. Ertl, Surf. Sci. 138 (1984) 505.
[3] M.R. Bassett, R. Imbihl, J. Phys. Chem. 93 (1990) 811.
[4] M. Rebholz, R. Prins, N. Kruse, Surf. Sci. 269/270 (1992) 293.
[5] K.A. Peterlinz, S.J. Sibener, J. Phys. Chem. 99 (1995) 2817.
[6] V.A. Bondzie, P. Kleban, D.J. Dwyer, Surf. Sci. 347 (1996) 319.
[7] A. von Oertzen, A. Mikhailov, H.-H. Rotermund, G. Ertl, Surf. Sci. 350 (1996) 259.
[8] N.M.H. Janssen, A. Schaak, B.E. Nieuwenhuys, R. Imbihl, Surf. Sci. 364 (1996) L555.
[9] D.G. Castner, G.A. Somorjai, Appl. Surf. Sci. 6 (1980) 29.
[10] C.S. Fadley, in: R.Z. Bachrach (Ed.), Synchrotron Radiation Research: Advances in Surface Science, Plenum, New York, 1989, chapter 9.
[11] D. Naumovic, A. Stuck, T. Greber, J. Osterwalder, L. Schlapbach, Surf. Sci. 269/270 (1992) 719.
[12] J. Osterwalder, P. Aebi, R. Fasel, D. Naumovic, P. Schwaller, T.J. Kreutz, L. Schlapbach, T. Abukawa, S. Kono, Surf. Sci. 331–333 (1995) 1002.
[13] T. Greber, O. Raetzo, T.J. Kreutz, P. Schwaller, W. Deichmann, E. Wetli, J. Osterwalder, Rev. Sci. Instrum. 68 (1997) 4549.
[14] M.P. Seah, W.A. Dench, Surf. Interf. Anal. 1 (1979) 2.
[15] S. Schwegmann, H. Over, V. De Renzi, G. Ertl, Surf. Sci. 375 (1997) 91.
[16] H. Xu, K.Y.S. Ng, Surf. Sci. 375 (1997) 161.
[17] V. Ganduglia-Pirovano, personal communication.
[18] J. Osterwalder, T. Greber, A. Stuck, L. Schlapbach, Phys. Rev. B 44 (1991) 13764.
[19] M. Seelmann-Eggebert, H.J. Richter, Phys. Rev. B 43 (1991) 9578.
[20] D. Naumovic, A. Stuck, T. Greber, J. Osterwalder, L. Schlapbach, Phys. Rev. B 47 (1993) 7462.
[21] S. Hüfner, J. Osterwalder, T. Greber, L. Schlapbach, Phys. Rev. B 42 (1990) 7350.
[22] T. Greber, J. Wider, E. Wetli, J. Osterwalder, Phys. Rev. Lett. 81 (1998) 1654.
[23] R. Fasel, P. Aebi, J. Osterwalder, L. Schlapbach, Surf. Sci. 331–333 (1995) 80.
[24] D.J. Friedman, C.S. Fadley, J. Electron Spectrosc. Relat. Phenom. 51 (1990) 689.